

Joint Detection and Super-Resolution Estimation of Multipath Signal Parameter Using Incremental Automatic Relevance Determination

Dmitriy Shutin and Nicolas Schneckenburger

Abstract

The presented work investigates a sparse Bayesian incremental automatic relevance determination (IARD) algorithm in the context of multipath parameter estimation in a super-resolution regime. The corresponding estimation problem is highly nonlinear and, in general, requires an estimation of the number of multipath components. In the IARD approach individual multipath components are processed sequentially, which permits a tractable convergence analysis of the corresponding inference expressions. This leads to a simple condition, termed here a pruning condition, that determines if a multipath component is “sparsified” or retained in the model, thus realizing a sparse estimator and permitting a fast and adaptive realization of the estimation algorithm. Yet previous experiments demonstrated that IARD fails to select the correct number of components when the parameters entering nonlinearly the multipath model are also estimated. To understand this effect, an analysis of the statistical structure of the pruning condition from the perspective of statistical hypothesis testing is proposed. It is shown that the corresponding test statistic in the pruning condition follows an extreme value distribution. As a result, when applied to the problem of multipath estimation, the standard IARD algorithm implements a statistical test with a very high probability of false alarm. This leads to insertion of estimation artifacts and underestimation of signal sparsity. Moreover, the probability of false alarm worsens as the number of measured signal samples grows. Based on the developed statistical interpretation of the IARD, an optimal adjustment of the pruning condition is proposed. This permits a reliable and efficient removal of estimation artifacts and joint estimation of signal parameters, as well as optimal model order selection within a sparse Bayesian learning framework. The presented experiments demonstrate the effectiveness of this approach.

Index Terms

Super-resolution channel estimation, model order selection, sparse Bayesian learning.

I. INTRODUCTION

Multipath propagation is known to have a significant impact on the performance of wireless communication or localization systems. However, when the multipath channel structure is known, it can offer a key to a reliable high-rate data communication or accurate localisation.

Typically, a multipath wireless channel is assumed to consist of a linear combination of a finite number of L discrete propagation paths, which we term multipath components, embedded in a white additive ambient noise and a non-white random process that represents diffuse propagation. While multipath components can be deterministically described by a set of parameters – dispersion parameters that characterize specular waves propagating from the transmitter site to the receiver site, such as a propagation delay, direction of departure, direction of arrival, and a Doppler frequency – diffuse components are of a random nature and are characterized statistically [1], [2], [3]. In this work we are concerned with an estimation of the discrete multipath components as they are a very sought-after characteristic of a wireless propagation channel due to their direct relationship to the geometry of the propagation environment.

Historically, the problem of multipath component parameter estimation has been solved using a combination of two techniques: super-resolution (SR) parameter estimation algorithms (see e.g., [2], [4], [5] and references therein) and model order selection [6], [7], [8]. Parameter estimation algorithms are used to find the parameters of multipath components given measurement data and a model of a multipath channel with a known number of superimposed components. SR property of the estimation algorithm is essential, as an accurate estimation of component parameters beyond bandwidth resolution is often required. Expectation-Maximization (EM) type of algorithms [2], [4], [9], [5] are often used for this purpose. They allow simplifying the numerical optimization of the objective function with respect to the dispersion parameters that enter the channel model nonlinearly. Unfortunately, these techniques are applicable only when the order of the model, i.e., the number of specular components is known – a requirement that is rarely satisfied in practice. This has motivated the use of model order selection techniques, such as Bayesian Information criterion or Minimum description length and similar [10], [7], [6], [8] to determine the number of components in the model. These methods select the model order by balancing the model complexity, i.e., a total number of parameters to be estimated, with a norm of the residual error. Yet for the considered problem these algorithms become computationally very

demanding: in order to find the optimal model order, the parameters of models with different number of components have to be estimated first, and then compared using selected criterion. In practice, the number of components can range from a only a few to several tens of components, making separate parameter estimation and model order selection very inefficient, especially in time-varying scenarios, where the number of components can change [11], [12].

To make estimation more efficient, we propose a variational Bayesian wireless channel estimator that combines model order selection and parameter estimation within a single framework. The proposed solution is based on merging a variational Bayesian parameter estimation [13], [14], which generalizes classical EM-based SR parameter estimation algorithms, and sparse Bayesian learning (SBL) techniques [15], [16], [17]. Sparse reconstruction of a multipath channel can effectively solve the model order selection problem, since irrelevant multipath components will be “sparsified” by the algorithm; sparsity, thus, effectively controls the complexity of the estimated models.

Such multipath estimation approaches have been to some extent explored in [18] and [19]. In [18] the authors casted the Space Alternating Generalized Expectation-Maximization (SAGE) algorithm for multipath parameter estimation¹ in a variational Bayesian framework. The new algorithm, termed variational Bayesian SAGE (VB-SAGE), introduces sparsity priors to jointly estimate model order via sparsity penalization and estimate the parameters of multipath components. The VB-SAGE algorithm makes a typical assumption on the independence of individual components. In [19] this assumption is relaxed by considering correlations between the gains of propagation paths. By adopting a special class of SBL algorithms, known as incremental Automatic Relevance Determination (IARD) [21], [22], [23], [24], a new algorithm is proposed that, as we will show here, generalizes the VB-SAGE algorithm. A key feature of both VB-SAGE and IARD algorithms is the structure of variational inference expressions that leads to a simple numerical condition for removing or keeping a component in the model. It is this condition that eventually leads to sparse estimate. Further in the text we refer to this condition as a pruning condition. The pruning condition permits the reduction of the model complexity “on the fly”, while the components are updated. In this way model order selection and parameter estimation are realized jointly.

It has been observed, however, that some of the estimated multipath components have small, yet non-zero weights [18]. In other words, the IARD and VB-SAGE estimators compress the measured signal, but overestimate the model order. To cancel erroneous components an empirical threshold was adopted in [24], [18], [22]. The selection of the threshold exploits the link between the pruning condition and an

¹See [20] and [5] for the details on the SAGE algorithm.

estimate of the per-component signal-to-noise ratio (SNR). Yet it remains unclear whether a particular choice of the threshold can be motivated more formally. A better understanding of these aspects can be exploited not only for improving performance of IARD schemes in the presence of noise and better understanding of the IARD performance in general, but for an accurate and fast extraction of specular multipath components, as we argue in this paper.

Thus, our goals in this work can be formulated as follows: we aim to further the theoretical understanding of IARD within the context of sparse estimation of multipath component and present a more detailed analysis of the pruning condition used in the IARD algorithms. Specifically, we show that the IARD algorithm generalizes VB-SAGE. Also, we demonstrate that the pruning condition used in IARD is equivalent to a statistical hypothesis test applied to a specific multipath component under the assumption that the other multipath components are fixed. With this new interpretation it becomes possible to show that (i) within the IARD scheme the presence of a component in the model can be determined using a statistical hypothesis test of a desired test size, (ii) the test is a uniformly most powerful (UMP), (iii) probability of false alarm for this test (i.e., the probability of falsely accepting a component in the model) is upper-bounded, with the standard IARD algorithm implementing the test with the highest probability of false alarm.

Throughout this paper we shall make use of the following notation. Vectors are represented as boldface lowercase letters, e.g., \mathbf{x} , and matrices as boldface uppercase letters, e.g., \mathbf{X} . For vectors and matrices $(\cdot)^H$ denotes the Hermitian transpose. We write $[\mathbf{X}]_{k,l}$ to denote an element of the matrix \mathbf{X} at the k th row and l th column. The expression $\text{diag}(\mathbf{x})$ stands for a diagonal matrix with the elements of \mathbf{x} on the main diagonal. For some positive-semidefinite matrix \mathbf{A} , notation $\|\mathbf{x}\|_{\mathbf{A}} = \sqrt{\mathbf{x}^H \mathbf{A} \mathbf{x}}$ denotes a weighted ℓ_2 norm of a vector \mathbf{x} . We write $\mathbb{E}_{q(x)} f(x)$ to denote the expectation of the function $f(x)$ under the probability density function $q(x)$. Finally, for a random vector \mathbf{x} , $\text{CN}(\mathbf{x}|\mathbf{a}, \mathbf{B})$ denotes a circular complex multivariate Gaussian pdf with mean \mathbf{a} and covariance matrix \mathbf{B} ; similarly, for a random variable x , $\text{Ga}(x|a, b) = \frac{b^a}{\Gamma(a)} x^{a-1} \exp(-bx)$ denotes a gamma pdf with parameters a and b .

II. SIGNAL MODEL

In the following sections we outline the used signal model. Also, the corresponding probabilistic formulation of the inference problem that builds the foundation for the variational Bayesian parameter estimation adopted here is presented.

A. Multipath channel model

Consider for simplicity a single-input–single-output (SISO) wireless channel². The received signal $y(t)$ can be represented as a superposition of an unknown number L of specular multipath components $w_l s(t; \boldsymbol{\theta}_l)$ contaminated by additive noise $\xi(t)$ (see e.g., [2], [18], [25]):

$$y(t) = \sum_{l=1}^L w_l s(t; \boldsymbol{\theta}_l) + \xi(t). \quad (1)$$

In (1) w_l is a complex-valued multipath gain and $s(t; \boldsymbol{\theta}_l)$ is an altered version of some transmitted signal $x(t)$. The alteration process is described by a (non-linear) mapping $x(t) \mapsto s(t; \boldsymbol{\theta}_l)$, where $\boldsymbol{\theta}_l$ is the vector of dispersion parameters, e.g., relative delay, Doppler shift, etc. For a SISO channel, $s(t; \boldsymbol{\theta}_l)$ can be represented as $s(t; \boldsymbol{\theta}_l) \equiv s(t; \tau_l, \nu_l) = e^{j2\pi\nu_l t} x(t - \tau_l)$, where $\boldsymbol{\theta}_l = [\tau_l, \nu_l]^T$, τ_l is a delay of the l th multipath component and ν_l is its Doppler shift. In general, the nonlinear mapping $x(t) \mapsto s(t; \boldsymbol{\theta}_l)$ also includes the measurement system effects, e.g., signal distortions at the transmitter and the receiver due to analog filtering, RF components, etc. Additive noise $\xi(t)$ is assumed to be a zero-mean wide-sense stationary Gaussian process. In addition to white noise, this term will also include effects due to diffuse scattering [2], [3].

In practice the signal $y(t)$ is sampled with the sampling period T_s , resulting in N discrete measurement samples. By stacking the samples in a vector $\mathbf{y} = [y(0), \dots, y((N-1)T_s)]^T$, model (1) can be rewritten in a more convenient matrix form as

$$\mathbf{y} = \sum_{l=1}^L w_l \mathbf{s}(\boldsymbol{\theta}_l) + \boldsymbol{\xi} = \mathbf{S}(\boldsymbol{\Theta})\mathbf{w} + \boldsymbol{\xi}, \quad (2)$$

where we define $\mathbf{s}(\boldsymbol{\theta}_l) = [s(0; \boldsymbol{\theta}_l), \dots, s((N-1)T_s; \boldsymbol{\theta}_l)]^T$, $\boldsymbol{\Theta} = [\boldsymbol{\theta}_1, \dots, \boldsymbol{\theta}_L]$, $\mathbf{w} = [w_1, \dots, w_L]^T$, and $\mathbf{S}(\boldsymbol{\Theta}) = [\mathbf{s}(\boldsymbol{\theta}_1), \dots, \mathbf{s}(\boldsymbol{\theta}_L)]$. The term $\boldsymbol{\xi} = [\xi(0), \dots, \xi((N-1)T_s)]^T$ is the additive noise vector that follows a circular complex normal distribution with covariance matrix $\mathbb{E}\{\boldsymbol{\xi}\boldsymbol{\xi}^H\} = \mathbf{\Lambda}^{-1}$. In the following we will assume that $\mathbf{\Lambda}$ is known or has been estimated; the estimation of diffuse scattering statistics and white noise statistics we will leave outside the scope of this work.

B. Probabilistic structure of the multipath channel model

Expression (2) is the starting point for the multipath parameter estimation algorithms. Given (2), the joint model order selection and parameter estimation aims at determining the values of L , \mathbf{w} ,

²The proposed method can also be extended to MIMO time-variant channels with stationary propagation constellation. This will, however, lead to a more complicated signal model with additional dispersion parameters, while not adding any new aspect relevant to the understanding of the proposed methods.

and Θ . For fixed L both \mathbf{w} and Θ can be found using classical maximum a posteriori (or maximum likelihood) approach, which amounts to a numerical maximization of the corresponding probability density function (pdf) $p(\mathbf{w}, \Theta | \mathbf{y}) \propto p(\mathbf{y} | \mathbf{w}, \Theta) p(\mathbf{w}, \Theta)$, where $p(\mathbf{y} | \mathbf{w}, \Theta) = \text{CN}(\mathbf{y} | \mathbf{S}(\Theta) \mathbf{w}, \Lambda^{-1})$ following (2). Unfortunately, in majority of practical cases the number of multipath components L is not known. A possible approach to circumvent an explicit specification of the model order consists of imposing sparsity constraints on \mathbf{w} . The advantage of such approach is a joint model order selection and parameter estimation within a Bayesian inference framework, as will be outlined below.

A classical SBL approach [15], [16], [17] assumes a hierarchical factorable prior $p(\mathbf{w} | \boldsymbol{\alpha}) p(\boldsymbol{\alpha}) = \prod_{l=1}^L p(w_l | \alpha_l) p(\alpha_l)$ for the weights \mathbf{w} , where $p(w_l | \alpha_l) = \text{CN}(w_l | 0, \alpha_l^{-1})$. Parameters α_l , also called sparsity parameters, regulate the width of this pdf and must be estimated along with the other model parameters – an approach referred to as *empirical Bayes*.

In IARD version of SBL two techniques are combined. First, the hyperprior $p(\boldsymbol{\alpha})$ is assumed to be non-informative by selecting $p(\boldsymbol{\alpha}) \propto \prod_{l=1}^L \alpha_l^{-1}$. Such choice is known as automatic relevance determination (ARD). The resulting inference scheme is then similar to a weighted version of minimum ℓ_1 -norm regression and basis pursuit denoising (see [26], [27], [28]) – more traditional “non-Bayesian” methods for learning sparse representations. Second, in the incremental inference approach to the SBL the corresponding objective function is optimized with respect to the parameters of one component per single algorithm iteration. Such incremental optimization permits a fast estimation of sparsity parameters [21], [22], [23]. Moreover, it also underlies the EM-based multipath estimation schemes, since it simplifies nonlinear optimizations with respect to dispersion parameters Θ . This motivates a combination of IARD and multipath inference schemes in a single framework.

The joint multipath parameter estimation and model order selection within IARD amounts to inference of the joint posterior pdf

$$p(\mathbf{w}, \Theta, \boldsymbol{\alpha} | \mathbf{y}) \propto p(\mathbf{y} | \mathbf{w}, \Theta) p(\mathbf{w} | \boldsymbol{\alpha}) p(\boldsymbol{\alpha}) p(\Theta), \quad (3)$$

where we explicitly assume that $p(\mathbf{w}, \Theta, \boldsymbol{\alpha}) = p(\mathbf{w} | \boldsymbol{\alpha}) p(\boldsymbol{\alpha}) p(\Theta)$. Unfortunately, (3) cannot be evaluated in closed form, but can be approximated using, e.g., variational Bayesian techniques [14], [13]. The latter aims at estimating an approximating pdf $q(\mathbf{w}, \Theta, \boldsymbol{\alpha})$ by maximizing the lower bound of the log-evidence $\log p(\mathbf{y})$:

$$\log p(\mathbf{y}) \geq \mathbb{E}_{q(\mathbf{w}, \Theta, \boldsymbol{\alpha})} \log \frac{p(\mathbf{w}, \Theta, \boldsymbol{\alpha}, \mathbf{y})}{q(\mathbf{w}, \Theta, \boldsymbol{\alpha})}, \quad (4)$$

which is equivalent to minimizing the Kullback-Leibler divergence between $q(\mathbf{w}, \Theta, \boldsymbol{\alpha})$ and the intractable

$p(\mathbf{w}, \Theta, \alpha | \mathbf{y})$. The complexity of the inference depends on the choice of $q(\mathbf{w}, \Theta, \alpha)$. Here we will assume that

$$q(\mathbf{w}, \Theta, \alpha) = q(\mathbf{w}) \prod_{k=1}^L q(\theta_k) q(\alpha_k). \quad (5)$$

Let us now specify each factor in (5). First, we will select $q(\theta_l) = \delta(\theta_l - \hat{\theta}_l)$. This assumption results in a point estimate of the dispersion parameters. This choice simplifies the numerical optimization of the right-hand side of (4). For the factor $q(\mathbf{w})$ we will consider two assumptions:

$$(A1) : \quad q(\mathbf{w}) = \prod_{l=1}^L q(w_l) = \prod_{l=1}^L \text{CN}(w_l | \hat{w}_l, \hat{\Phi}_l), \quad (6)$$

$$(A2) : \quad q(\mathbf{w}) = \text{CN}(\mathbf{w} | \hat{\mathbf{w}}, \hat{\Phi}). \quad (7)$$

A1 explicitly enforces a statistical independence between individual multipath components; this assumption underlies the SAGE [5] and the VB-SAGE algorithms [18] for multipath parameter estimation. Under the assumption A2 the gains of the components are assumed to be correlated. This formulation is used in a classical SBL and in the IARD algorithm for multipath estimation in [19]. In the following we will consider both assumptions and investigate their impact on multipath estimation and detection. Let us mention here that A1 can be obtained as a special case of A2 by constraining $\hat{\Phi}$ to a diagonal matrix. The form of the factor $q(\alpha)$ can be obtained analytically as a maximizer of (4) for the chosen form of $q(\theta_l)$ and $q(\mathbf{w})$. For the IARD case it can be shown [18], [22] that

$$q(\alpha) = \prod_{l=1}^L q(\alpha_l) = \prod_{l=1}^L \text{Ga}(\alpha_l; 1, \hat{\alpha}_l^{-1}),$$

i.e., $q(\alpha_l)$ is parameterized by a single coefficient $\hat{\alpha}_l$.

The maximization of the bound in (4) then reduces to the estimation of the parameters $\hat{\mathbf{w}}$, $\hat{\Phi}$, $\hat{\alpha}_l$, and $\hat{\theta}_l$, $l = 1, \dots, L$ that parameterize (5). In what follows we describe this in more details.

C. Incremental variational inference of model parameters

The IARD algorithm optimizes (4) with respect to the parameters of one component per iteration, cycling through the components in a round-robin fashion. Consider now the variational inference steps for a single component l . We will begin with the estimation of $q(\theta_l)$. To this end we define $\Theta_{-l} = [\theta_1, \dots, \theta_{l-1}, \theta_{l+1}, \dots, \theta_L]$ as a set of dispersion parameters obtained by removing θ_l from Θ , and

assume that the pdfs $q(\mathbf{w})$, $q(\alpha)$, and $q(\Theta_{-l})$ are available.³ The bound in (4) on $\log p(\mathbf{y})$ with respect to $q(\theta_l)$ can then be expressed as $\log p(\mathbf{y}) \geq \mathbb{E}_{q(\theta_l)} \log (\tilde{p}(\theta_l)/q(\theta_l))$, where

$$\tilde{p}(\theta_l) \propto \exp\left(\mathbb{E}_{q(\mathbf{w}, \Theta_{-l})} \log p(\mathbf{y}|\mathbf{w}, \Theta) p(\Theta)\right). \quad (8)$$

This bound is maximized when the Kullback-Leibler divergence between $q(\theta_l)$ and $\tilde{p}(\theta_l)$ is minimal. Due to the assumed form of $q(\theta_l)$, this is achieved when $\hat{\theta}_l$ is aligned with the mode of $\tilde{p}(\theta_l)$. By computing the expectation in (8) it can be shown that

$$\begin{aligned} \hat{\theta}_l = \operatorname{argmax}_{\theta_l} & \left\{ \log p(\theta_l) - \|\mathbf{r}_l - \hat{w}_l \mathbf{s}(\theta_l)\|_{\Lambda}^2 \right. \\ & \left. - \sum_{k=1, k \neq l}^L 2\Re \left\{ [\hat{\Phi}]_{k,l} \mathbf{s}(\hat{\theta}_k)^H \Lambda \mathbf{s}(\theta_l) \right\} - [\hat{\Phi}]_{l,l} \|\mathbf{s}(\theta_l)\|_{\Lambda}^2 \right\}, \end{aligned} \quad (9)$$

where $\Re\{\cdot\}$ denotes the real part operator and

$$\mathbf{r}_l = \mathbf{y} - \sum_{k=1, k \neq l}^L \hat{w}_k \mathbf{s}(\hat{\theta}_k) \quad (10)$$

is a residual signal that cancels the contribution of the other $L - 1$ components. Solving (9) requires in general a numerical optimization. Let us point out that the last two terms in (9) account for correlations between the elements of \mathbf{w} , acting as penalty factors in the estimator of θ_l . Also, note that under the assumption A1 (9) coincides with the estimation expression used in the VB-SAGE algorithm [18].

Now, let us consider the estimation of $q(\alpha_l)$. The bound in (4) with respect to $q(\alpha_l)$ can be expressed as $\log p(\mathbf{y}) \geq \mathbb{E}_{q(\alpha_l)} \log \tilde{p}(\alpha_l)/q(\alpha_l)$, where

$$\tilde{p}(\alpha_l) \propto \exp\left(\mathbb{E}_{q(\mathbf{w})} \log p(w_l|\alpha_l) p(\alpha_l)\right).$$

It has been demonstrated in [18] (for the assumption A1) and in [22] (for the assumption A2) that the sequence of estimates $\{q^{[0]}(\alpha_l), q^{[1]}(\alpha_l), q^{[2]}(\alpha_l), \dots\}$, obtained by repeated maximization of the right-hand side of (4) with respect to the pdfs $q(w_l)$ and $q(\alpha_l)$ (for A1), or $q(\mathbf{w})$ and $q(\alpha_l)$ (for A2), converges to the pdf $q^{[\infty]}(\alpha_l) = \text{Ga}(\alpha_l|1, (\hat{\alpha}_l^{[\infty]})^{-1})$ with

$$\hat{\alpha}_l^{[\infty]} = \begin{cases} (|\mu_l|^2 - \varsigma_l)^{-1}, & \frac{|\mu_l|^2}{\varsigma_l} > 1 \\ \infty, & \frac{|\mu_l|^2}{\varsigma_l} \leq 1. \end{cases} \quad (11)$$

³In other words, we assume that the parameters of the corresponding pdfs are known.

The parameters ς_l and μ_l in (11) are computed as follows. For the assumption A1:

$$(A1) : \quad \varsigma_l = 1/\|\mathbf{s}(\hat{\boldsymbol{\theta}}_l)\|_{\Lambda}^2, \quad \mu_l = \varsigma_l \mathbf{s}(\hat{\boldsymbol{\theta}}_l)^H \boldsymbol{\Lambda} \bar{\mathbf{r}}_l^{[A1]},$$

$$\bar{\mathbf{r}}_l^{[A1]} = \mathbf{y} - \sum_{k=1, k \neq l}^L \hat{w}_k \mathbf{s}(\hat{\boldsymbol{\theta}}_k). \quad (12)$$

For the assumption A2, we first define

$$\hat{\mathbf{A}}_{-l} = \text{diag}([\hat{\alpha}_1, \dots, \hat{\alpha}_{l-1}, \hat{\alpha}_{l+1}, \dots, \hat{\alpha}_L]),$$

$$\mathbf{S}(\hat{\boldsymbol{\Theta}}_{-l}) = [\mathbf{s}(\hat{\boldsymbol{\theta}}_1), \dots, \mathbf{s}(\hat{\boldsymbol{\theta}}_{l-1}), \mathbf{s}(\hat{\boldsymbol{\theta}}_{l+1}), \dots, \mathbf{s}(\hat{\boldsymbol{\theta}}_L)],$$

$$\hat{\boldsymbol{\Phi}}_{-l} = \left(\mathbf{S}(\hat{\boldsymbol{\Theta}}_{-l})^H \boldsymbol{\Lambda} \mathbf{S}(\hat{\boldsymbol{\Theta}}_{-l}) + \hat{\mathbf{A}}_{-l} \right)^{-1}, \quad (13)$$

$$\hat{w}_{-l} = \hat{\boldsymbol{\Phi}}_{-l} \mathbf{S}(\hat{\boldsymbol{\Theta}}_{-l})^H \boldsymbol{\Lambda} \mathbf{y}, \text{ and}$$

$$\bar{\mathbf{r}}_l^{[A2]} = \mathbf{y} - \mathbf{S}(\hat{\boldsymbol{\Theta}}_{-l}) \hat{w}_{-l}.$$

Then, ς_l and μ_l for this assumption are evaluated as follows

$$(A2) : \quad \varsigma_l = \left(\mathbf{s}(\hat{\boldsymbol{\theta}}_l)^H \boldsymbol{\Lambda} \mathbf{s}(\hat{\boldsymbol{\theta}}_l) - \right.$$

$$\left. \mathbf{s}(\hat{\boldsymbol{\theta}}_l)^H \boldsymbol{\Lambda} \mathbf{S}(\hat{\boldsymbol{\Theta}}_{-l}) \hat{\boldsymbol{\Phi}}_{-l} \mathbf{S}(\hat{\boldsymbol{\Theta}}_{-l})^H \boldsymbol{\Lambda} \mathbf{s}(\hat{\boldsymbol{\theta}}_l) \right)^{-1},$$

$$\mu_l = \varsigma_l \mathbf{s}(\hat{\boldsymbol{\theta}}_l)^H \boldsymbol{\Lambda} \mathbf{y} -$$

$$\varsigma_l \mathbf{s}(\hat{\boldsymbol{\theta}}_l)^H \boldsymbol{\Lambda} \mathbf{S}(\hat{\boldsymbol{\Theta}}_{-l}) \hat{\boldsymbol{\Phi}}_{-l} \mathbf{S}(\hat{\boldsymbol{\Theta}}_{-l})^H \boldsymbol{\Lambda} \mathbf{y} \quad (14)$$

$$= \varsigma_l \mathbf{s}(\hat{\boldsymbol{\theta}}_l)^H \boldsymbol{\Lambda} (\mathbf{y} - \mathbf{S}(\hat{\boldsymbol{\Theta}}_{-l}) \hat{w}_{-l})$$

$$= \varsigma_l \mathbf{s}(\hat{\boldsymbol{\theta}}_l)^H \boldsymbol{\Lambda} \bar{\mathbf{r}}_l^{[A2]}.$$

Let us point out that for both A1 and A2 cases, the weight μ_l is a projection of $\mathbf{s}(\hat{\boldsymbol{\theta}}_l)$ on the corresponding residual signal $\bar{\mathbf{r}}_l^{[A1]}$ or $\bar{\mathbf{r}}_l^{[A2]}$, respectively. The latter are computed by canceling (subtracting) the contribution of the other $L-1$ components. Note that $\bar{\mathbf{r}}_l^{[A1]}$ coincides with (10); also, $\bar{\mathbf{r}}_l^{[A2]}$ and $\bar{\mathbf{r}}_l^{[A1]}$ are equal when $\hat{\boldsymbol{\Phi}}_{-l}$ is diagonal, i.e., for uncorrelated components. This will be a valid assumption for components that are physically well separated, i.e., when $\mathbf{s}(\boldsymbol{\theta}_l)^H \boldsymbol{\Lambda} \mathbf{s}(\boldsymbol{\theta}_k) \approx 0$, $k \neq l$. Thus, for uncorrelated components the IARD and the VB-SAGE algorithms will lead to the same estimation results. Also, when assumption \mathcal{A}_{∞} is used with IARD, an instance of the VB-SAGE algorithm is obtained. Yet IARD does not require an introduction of any latent variables, as it was done in the VB-SAGE algorithm.

Finally, we estimate $q(w_l)$ and $q(\mathbf{w})$. For the assumption A1 the parameters of $q(w_l)$ are computed as

$$\hat{\Phi}_l = \left(\|\mathbf{s}(\hat{\boldsymbol{\theta}}_l)\|_{\Lambda}^2 + \hat{\alpha}_l^{[\infty]} \right)^{-1}, \hat{w}_l = \hat{\Phi}_l \mathbf{s}(\hat{\boldsymbol{\theta}}_l)^H \Lambda \bar{\mathbf{r}}_l^{[A1]}. \quad (15)$$

Similarly, for the assumption A2 we compute

$$\begin{aligned} \hat{\Phi} &= \left(\mathbf{S}(\hat{\Theta})^H \Lambda \mathbf{S}(\hat{\Theta}) + \text{diag}(\hat{\boldsymbol{\alpha}}) \right)^{-1}, \\ \hat{\mathbf{w}} &= \hat{\Phi} \mathbf{S}(\hat{\Theta})^H \Lambda \mathbf{y}, \end{aligned} \quad (16)$$

where $\hat{\boldsymbol{\alpha}} = [\hat{\alpha}_1, \dots, \hat{\alpha}_{l-1}, \hat{\alpha}_l^{[\infty]}, \hat{\alpha}_{l+1}, \hat{\alpha}_L]^T$.

The key advantages of such incremental component-wise estimation scheme are the expressions (9) and (11). The former permits a simpler numerical optimization of the dispersion parameters as the dimensionality of the resulting objective function equals to the dimensionality of $\boldsymbol{\theta}_l$, rather than that of Θ . Result (11) gives a simple criterion for model order selection: when $|\mu_l|^2 \leq \varsigma_l$, we get $\hat{\alpha}_l^{[\infty]} = \infty$, i.e., $w_l \rightarrow 0$ and the component is removed. This implements an automatic model order selection. Moreover, the signal model can be constructed from bottom up, i.e., starting with an empty model $\mathbf{S}(\hat{\Theta})\hat{\mathbf{w}} = \mathbf{0}$, and initializing the first component using ‘‘incoherent’’ initialization as described in the Algorithm (1).

Algorithm 1 Component initialization

Compute $\mathbf{r}_l \leftarrow \mathbf{y} - \mathbf{S}(\hat{\Theta})\hat{\mathbf{w}}$; estimate $\boldsymbol{\theta}_l$ using

$$\hat{\boldsymbol{\theta}}_l = \underset{\boldsymbol{\theta}_l}{\text{argmax}} \left\{ \log p(\boldsymbol{\theta}_l) - \|\mathbf{r}_l^H \mathbf{s}(\boldsymbol{\theta}_l)\|_{\Lambda}^2 \right\}, \quad (17)$$

Compute $q(\alpha_l)$ using (11)

if $\hat{\alpha}_l^{[\infty]}$ is finite **then**

 Compute $q(w_l)$ using (15) (or $q(\mathbf{w})$ using (16))

else

 Discard the component and abort initialization

end if

If during the initialization the test (11) results in a finite sparsity parameter $\hat{\alpha}_l^{[\infty]}$, a new component is accepted in the model. The parameters of the components are then updated following the Algorithm 2.

Algorithm 2 Parameter update

```

while Not converged do
  for  $l \in \{1, \dots, L\}$  do
    Update  $q(\boldsymbol{\theta}_l)$  from (9) and  $q(\alpha_l)$  using (11)
    if  $\hat{\alpha}_l^{[\infty]}$  is finite then
      Update  $q(w_l)$  using (15) (or  $q(\boldsymbol{w})$  using (16))
    else
      Remove the  $l$ th component from the model
    end if
  end for
end while

```

After update, the initialization can be repeated again for an updated residual signal. The algorithm is interrupted when no new components can be added to the model. Let us also mention at this stage that $\hat{\Phi}_{-l}$ can be efficiently computed using rank-one updates (see [18] for more details). Thus, $q(\boldsymbol{w})$ can be efficiently updated even for large L .

The condition $|\mu_l|^2 > \varsigma_l$ in (11) we term a pruning condition since it determines if $\hat{\alpha}_l^{[\infty]}$ is finite. It forms a basis for a multipath component detector. In fact, the sparsity of the estimated model is governed by this condition. To better understand its properties and limitations we consider this condition in more details in the following section.

III. ANALYSIS OF THE PRUNING CONDITION

Let us now investigate this pruning condition in greater detail for both A1 and A2 assumptions. To this end we define $\rho_l = |\mu_l|^2/\varsigma_l$. A closer look at (12) and (14) reveals that the parameters μ_l and ς_l correspond, respectively, to the posterior estimate of the l th path weight w_l and its variance when $\hat{\alpha}_l = 0$. Thus, we can interpret ρ_l as an estimate of the l th component SNR after the processing.⁴ Specifically, the pruning condition

$$\rho_l > 1, \tag{18}$$

states that an estimate of the approximating pdf $q(\alpha_l)$ has a finite mean if, and only if, an estimate of the l th component SNR after subtracting the interference of the other $L - 1$ components exceeds 1 (or

⁴This can also be interpreted as the component SNR after a matched filter processing, with $\boldsymbol{s}(\hat{\boldsymbol{\theta}}_l)$ playing the role of a matched filter.

equivalently 0 dB).

Yet in many practical applications a 0 dB threshold might not represent the desired level of confidence in the estimated component. Moreover, we have empirically observed the condition (18) generally overestimates the model order: some of the detected components were falsely introduced into the model, with the estimated weights having small, yet non-zero weights and the corresponding parameters ρ_l exceeding a 0 dB threshold. Empirical adjustment of the threshold to some level $\kappa_l \geq 1$ improves the model order estimate [24], [18], [22], [23]. In what follows we explain why signal sparsity is overestimated with the condition (18) and how to select the threshold κ_l such that the conditions $\rho_l > \kappa_l$ is more robust against estimation artifacts. For this purpose we will explore a connection between the statistical structure of (18) and hypothesis testing.

Consider a single component l , and assume that the parameters of the other components are fixed. Define now two hypotheses H_0 and H_1 for the “true” weight w_l of the l th multipath component as follows:

$$\begin{cases} H_0 : w_l = 0 \\ H_1 : w_l \neq 0. \end{cases} \quad (19)$$

Our goal here is to understand how statistics of ρ_l can be utilized to choose between these two hypotheses in the Neyman-Pearson sense. To this end we will consider the distribution of ρ_l under H_0 and H_1 hypotheses for both A1 and A2 assumptions.

A. Assumption A1: independent multipath components

We will begin our analysis with the following proposition:

Proposition 1. *Assume that $\hat{\theta}_l$ is found from (9) and that other factors in (6) are fixed. Then, under hypothesis H_0 the statistic ρ_l will follow an extreme value distribution [29] with the following pdf:*

$$p(\rho_l|H_0) = \begin{cases} (e^{-N/e})\delta(\rho_l) & 0 \leq \rho_l \leq 1 \\ (1 - e^{-N/e})\tilde{p}(\rho_l|H_0) & \rho_l > 1 \end{cases} \quad (20)$$

where $\delta(\rho_l)$ is a Dirac delta distribution and

$$\tilde{p}(\rho_l|H_0) = e^{(-\rho_l + \log(N) - e^{-\rho_l + \log(N)})}, \quad \rho_l \geq 0, \quad (21)$$

is a pdf of the Gumbel distribution [30].

Proof: Consider the distribution of ρ_l under the hypothesis H_0 for some arbitrary value of θ_l and

known noise statistics. Due to the efficiency of maximum likelihood estimators for linear models [31], it is straightforward to show that $\mu_l \sim \text{CN}(\mu_l|0, \varsigma_l)$. Recall now that $\rho_l = |\mu_l|^2/\varsigma_l$. It is known that the square of a normally distributed zero mean random variable normalized by its variance will follow a χ^2 distribution. Since the variance of real and imaginary parts of μ_l is $\varsigma_l/2$, then ρ_l will follow a scaled⁵ χ^2 distribution with two degrees of freedom. In our case it is an exponential distribution with the pdf

$$p(\rho_l) = e^{-\rho_l}, \quad \rho_l \geq 0. \quad (22)$$

This distribution arises when for a fixed θ_l different realizations of the residual signal $\bar{\mathbf{r}}_l^{[A1]}$ are generated. Alternatively, $\bar{\mathbf{r}}_l^{[A1]}$ can be fixed and θ_l then drawn at random. Note that under H_0 the residual $\bar{\mathbf{r}}_l^{[A1]}$ is a realization of an N -dimensional Gaussian noise vector. However, due to maximization (9) we select the “best” dispersion parameter $\hat{\theta}_l$ out of N independent possibilities.⁶ As a result an observed value of ρ_l under H_0 will follow the distribution of a maximum out of N values drawn from (22). Such type of distributions are known as extreme value distributions.

To derive the distribution function $F_{\max}(\rho_l)$ of the corresponding extreme value distribution, we apply the Fisher-Tippett-Gnedenko theorem [29] to the distribution function $F(\rho_l) = 1 - e^{-\rho_l}$ of the exponential pdf (22). By the theorem, $F_{\max}(\rho_l)$ can be computed as the limit of appropriately shifted and scaled variable ρ_l : $F_{\max}(\rho_l) = \lim_{n \rightarrow \infty} \left(F\left(\frac{\rho_l - b_n}{a_n}\right) \right)^n$ for some real sequences $a_n > 0$ and $b_n > 0$ that are independent of ρ_l . In our case, it can be demonstrated that for $a_n = 1$ and $b_n = \log(n)$, the maximum of out of N exponentially distributed values will follow a Gumbel distribution [30] $F_{\max}(\rho_l)$ with the distribution function

$$F_{\max}(\rho_l) = \exp\left(-e^{-(\rho_l - \log(N))}\right)$$

and the corresponding pdf

$$\tilde{p}(\rho_l|H_0) = e^{(-\rho_l + \log(N) - e^{-\rho_l + \log(N)})}, \quad \rho_l \geq 0. \quad (23)$$

Note, however, that for $\rho_l \leq 1$ the sparsity parameter $\hat{\alpha}_l^{[\infty]} = \infty$. In this case the hypothesis H_0 is automatically accepted. Taking this into consideration, the pdf $p(\rho_l|H_0)$ can be specified as

$$p(\rho_l|H_0) = \begin{cases} F_{\max}(1)\delta(\rho_l) & 0 \leq \rho_l \leq 1 \\ (1 - F_{\max}(1))\tilde{p}(\rho_l|H_0) & \rho_l > 1, \end{cases} \quad (24)$$

⁵The scaling factor in this case is 1/2 to compensate for the reduced variance of real and imaginary parts.

⁶Note that possible correlations in the residual signal due to diffuse multipath are “whitened” by the matrix $\mathbf{\Lambda}^{-1}$.

which completes the proof. ■

The next proposition defines the distribution of ρ_l under hypothesis H_1 .

Proposition 2. *Under hypothesis H_1 the statistic ρ_l will follow a scaled non-central chi-square distribution*

$$p(\rho_l|H_1) = \begin{cases} 0 & 0 \leq \rho_l \leq 1 \\ \frac{1}{Z} \tilde{p}(\rho_l|H_0) & \rho_l > 1 \end{cases} \quad (25)$$

where

$$\begin{aligned} \tilde{p}_{H_1}(\rho_l) &= e^{-(\rho_l + \frac{\eta_l}{2})} I_0\left(\sqrt{2\eta_l \rho_l}\right), \\ \text{and } Z &= \int_1^\infty \tilde{p}_{H_1}(\rho_l) d\rho_l. \end{aligned} \quad (26)$$

Proof: The distribution of ρ_l under hypothesis H_1 can be studied in a similar fashion. The weight μ_l will follow a Gaussian distribution with the true (unknown) mean $w_l \neq 0$ and a variance ς_l . Following the same line of arguments as for the H_0 case, it can be shown that ρ_l will follow a scaled non-central chi-square distribution $\chi^2_2(\eta_l)$ with two degree of freedom and a non-centrality parameter $\eta_l = 2|w_l|^2/\varsigma_l$:

$$\tilde{p}(\rho_l|H_1) = e^{-(\rho_l + \frac{\eta_l}{2})} I_0\left(\sqrt{2\eta_l \rho_l}\right), \quad \rho_l > 0, \quad (27)$$

where $I_0(x)$ is a modified Bessel function of the first kind. Since for $\rho_l \leq 1$ the H_1 hypothesis is automatically rejected, the support of $p(\rho_l|H_1)$ is restricted to the interval $(1, \infty)$. Taking this into account leads to result (25), which finalizes the proof. ■

Let us note that, strictly speaking, (25) will hold for components with a sufficiently high “true” SNR $|w_l|^2/\varsigma_l$. In high SNR regime optimization (9) will consistently result in the same value of $\hat{\theta}_l$. Yet as w_l decreases, the corresponding residual signal $\bar{r}_l^{[A1]}$ becomes dominated by the additive noise ξ and a mixture of (25) and (23) will be observed.

Now, we can select between H_0 and H_1 using the following test function $T(\rho_l)$:

$$T(\rho_l) = \begin{cases} 0, & \rho_l \leq \kappa_l \\ 1, & \rho_l > \kappa_l, \end{cases}, \quad (28)$$

$$\text{s.t. } \kappa_l > 0, \quad \mathbb{E}_{p(\rho_l|H_0)} \{T(\rho_l)\} = \epsilon_l,$$

where ϵ_l is the size of the test. Let us now indicate some important properties of $T(\rho_l)$.

- 1) The test (28) is uniformly most powerful (UMP) test of size ϵ_l to choose between H_0 and H_1 specified by pdfs (20) and (25), respectively. This follows from the fact that the rejection region

of the test function $T(\rho_l)$, given by the interval $[\log(1/\log(1 - \epsilon_l)^{-1/N}), \infty]$ is independent of η_l [32].

- 2) Under assumption A1 the standard IARD algorithm implements the test (28) with $\kappa_l = 1$, as seen from (11).
- 3) Since for $\rho_l \leq 1$ the corresponding component is automatically removed, the size ϵ_l of the test (28) must be upper bounded. The upper bound is given by $(1 - F_{\max}(1))$.

It is important to stress that for a standard threshold $\kappa_l = 1$, the size of the hypothesis test ϵ_l will be quite large for typical values of N (see Fig. 1). In other words the standard IARD will implement the test (28)

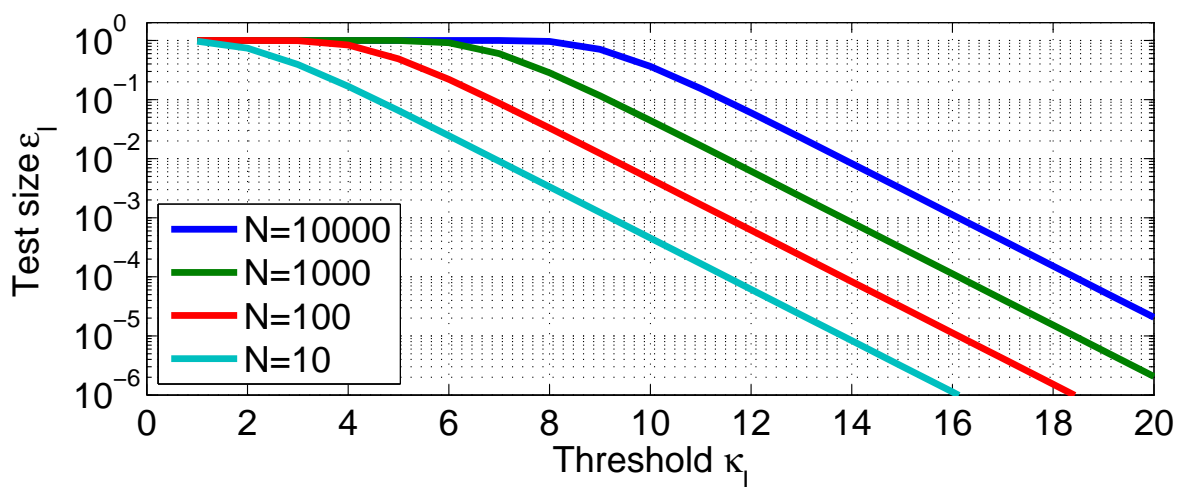


Fig. 1. Size ϵ_l of the test (28) versus threshold κ_l for different values of N .

with a very high probability of false alarm. As a result, H_0 will be falsely accepted more often, leading to estimation artifacts. Moreover, as the number of samples N increases, the probability of generating artifacts grows as well, making it more difficult to distinguish “true” components from noise. The reason for this is the optimization (9), which leads to the emergence of the extreme value distribution (20). As N increases, this distribution shifts further away from the standard threshold $\kappa_l = 1$, making the correct rejection of artifacts less probable. Naturally, by increasing the threshold κ_l we can control the probability of false detection at some desired level ϵ_l .

B. Assumption A2: correlated multipath components

Under the assumption A2 the pruning condition (18) has a similar interpretation. However, due to the correlations between the elements of \mathbf{w} , the corresponding analysis becomes significantly more involved.

Let us begin by considering the marginal posterior of w_l for the case when $\alpha_l = 0$. This is again a Gaussian pdf with the mean μ_l and the variance ς_l given by (14). Consider now the expectation $\mathbb{E}\{\mu_l\} = \mathbb{E}\{\varsigma_l \mathbf{s}_l(\hat{\boldsymbol{\theta}}_l)^H \boldsymbol{\Lambda} \bar{\boldsymbol{\tau}}_l^{[A2]}\}$ in (14). It can be shown that

$$\begin{aligned} \mathbb{E}\{\mu_l\} = & \varsigma_l \mathbf{s}_l(\boldsymbol{\theta}_l)^H \left(\boldsymbol{\Lambda}^{-1} + \mathbf{S}(\hat{\boldsymbol{\Theta}}_{-l}) \hat{\mathbf{A}}_{-l}^{-1} \mathbf{S}(\hat{\boldsymbol{\Theta}}_{-l})^H \right)^{-1} \\ & \times \mathbf{S}(\hat{\boldsymbol{\Theta}}_{-l}) \mathbf{w}_{-l} + w_l. \end{aligned} \quad (29)$$

where we re-used definitions (13) to simplify notation. By inspecting (29) we see that the bias $\mathbb{E}\{\mu_l\}$ does not vanish under hypothesis H_0 , i.e., when $w_l = 0$. Due to the correlations between the components, this bias is proportional to the “true” weights \mathbf{w}_{-l} , which are generally unknown. In other words, in order to decide between H_0 and H_1 within the incremental estimation approach, i.e., for a particular component l , we need to know the weights of the other multipath component. This in general prohibits a computation of the pdf $p_{H_0}(\rho_l)$ or $p_{H_1}(\rho_l)$ for the case A2 unless some assumptions about the true weights \mathbf{w}_{-l} can be made.

Nonetheless, our simulations show that the test (28) applied to the case A2 performs quite well.

IV. SIMULATIONS RESULTS

In the following we will investigate the performance of the proposed joint estimator and component detector for synthetic channels.

A. One component in noise

We will begin with a single synthetic multipath component in white noise, i.e., $L = 1$. For that we generate a channel response according to (2) with the following assumptions. We restrict the set of dispersion parameters to a single delay τ , so that $\mathbf{s}(\boldsymbol{\theta}) \equiv \mathbf{s}(\tau)$. The vector $\mathbf{s}(\tau)$ is constructed as $\mathbf{s}(\tau) = [s[-\tau/T_s], \dots, s[(N-1) - \tau/T_s]]^T$, where $N = 128$ and $T_s = 1$ s. The signal $s[n]$ is an OFDM signal with K subcarriers located at discrete frequencies $2\pi k/K$, $k = 0, \dots, K-1$. Each subcarrier is generated with a constant unit magnitude and random phase uniformly drawn from the interval $[0, 2\pi]$. The delay τ of the synthetic component is set to $\tau = 0$. The weight w has a unit magnitude and a random phase drawn from the interval $[0, 2\pi]$.

Our goal in this experiment is to validate the derived distributions of the decision statistic ρ_l for both H_0 and H_1 hypothesis. To this end we restrict the values of estimated component delays to the sampling instances. The estimation algorithm is then initialized with only 2 components: one with the delay set to the true delay τ to approximate the H_1 hypothesis, and the other one set to the neighboring sampling

instance to approximate the hypothesis H_0 . To collect the corresponding statistics, we run the algorithm and collect the values of ρ_1 and ρ_2 over 10000 independent runs of the algorithm. The obtained empirical distributions of both statistics are then compared to the derived theoretical distributions $p(\rho_l|H_0)$ and $p(\rho_l|H_1)$. For both components a pruning threshold of $\kappa_1 = \kappa_2 = 1$ is used, which corresponds to the standard IARD pruning condition. The analysis is performed for different input SNRs that we compute as $10 \log_{10} \|w_1 \mathbf{s}(\tau_1)\|^2 / \|\boldsymbol{\xi}\|^2 + 10 \log_{10}(N)$; here, $10 \log_{10}(N)$ is the processing gain of the estimator.

We begin our tests for the assumption A1. For that we use $K = N$, which corresponds to the correlation coefficient of 0.007 between the components with delays located at two neighboring sampling instances. In Fig. 2 we plot the resulting distributions for 9dB, 13dB, 17dB, and 21dB SNR. As we see, there is a very good fit between the empirical and theoretical distributions under the H_0 hypothesis. Also, as expected, for low SNR the derived pdf $p(\rho_l|H_1)$ deviates slightly from the observed empirical distribution.

Now, let us consider the same scenario, yet for correlated components. To increase the correlation between the components we select $K = N/2$, $K = N/4$, $K = N/8$, and $K = N/16$, which is equivalent to keeping the sampling rate fixed while reducing the bandwidth of the signals. This leads to increased correlation between closely spaced components. The correlation coefficients between two signals located at two consecutive delays for the above chosen values of K are 0.62, 0.89, 0.97, and 0.99, respectively.

In Fig. 3 we show the empirical distributions of the decision statistic for 17dB SNR and the corresponding pdfs $p(\rho_l|H_0)$ and $p(\rho_l|H_1)$. Note that the latter are computed under the assumption A1. As expected, for low correlations the pdfs derived for the assumption A1 provide a close approximation for the A2 case, both for H_0 and H_1 hypotheses. As the correlation increases, the pdfs of both hypotheses exhibit a second mode at the location of the alternative hypothesis. This is direct consequence of the high correlation between the components: depending on the noise realization, a component that is “marked” as an H_0 hypothesis fits the synthetic signal better than the one “marked” as an H_1 . Practically, it is, however, not important which component is eventually selected, as long as the artifacts are removed with an appropriately selected threshold κ_l . Considering the tails of the pdf $p(\rho_l|H_0)$ we can conclude that in the A2 case the threshold κ_l computed for the A1 assumption seem to be a reasonable practical approximation.

Let us now test the performance of the proposed detector with the adjusted threshold κ_l . For that we use the same simulation parameters: we generate a single component with $\tau = 0$, $N = 128$, and $T_s = 1$. As the performance measure we look at the number of estimated components and the empirical distribution of the estimated delay values versus SNR for the threshold $\kappa_l = 1$, i.e., no adjustment, and

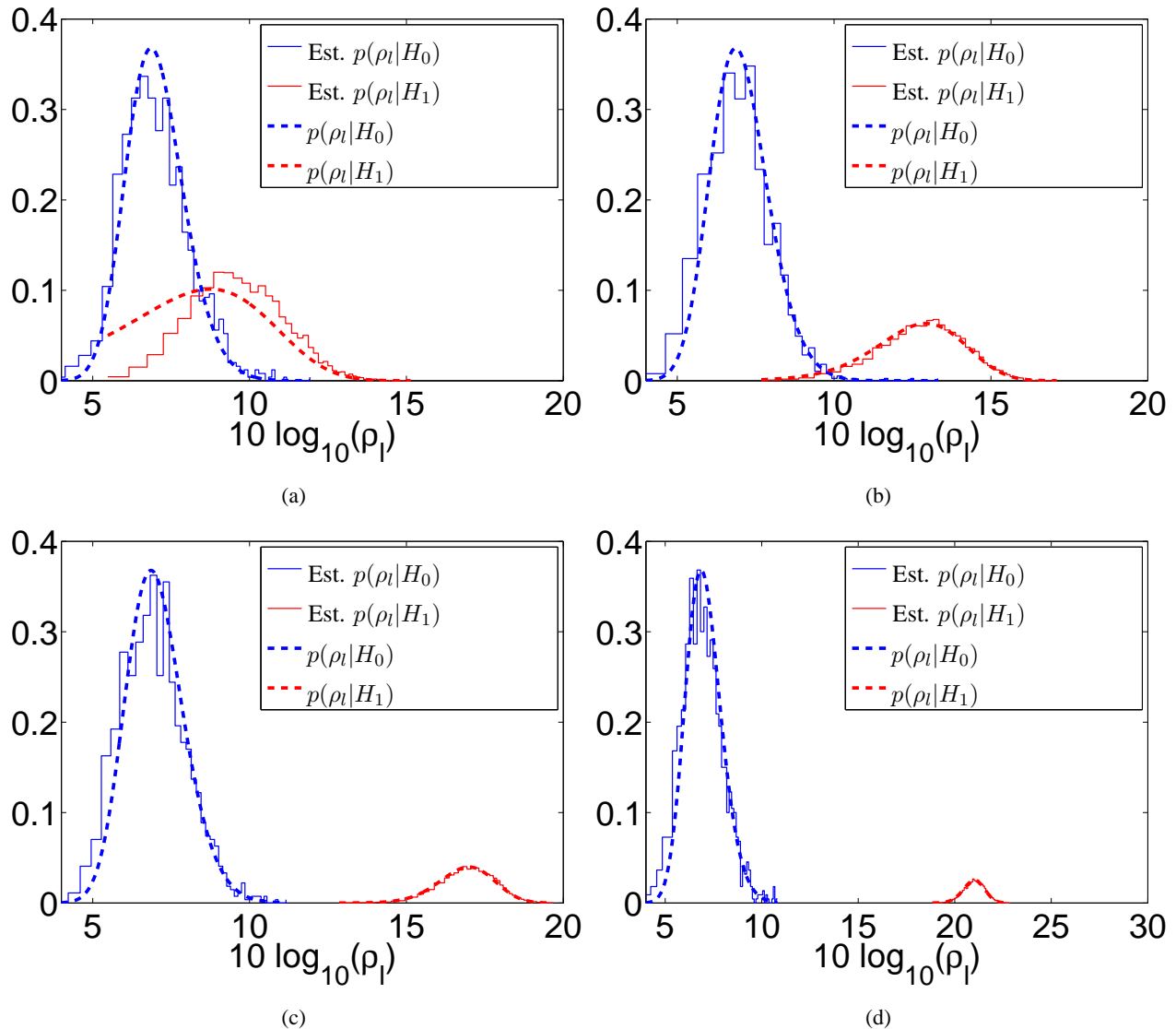


Fig. 2. Comparison of empirical and derived distributions of the test statistic ρ_l under H_0 and H_1 hypotheses for a) SNR = 9dB, b) SNR = 13dB, c) SNR = 17dB, and d) SNR = 21dB.

adjusted threshold

$$\kappa_l = \log(1/\log(1 - \epsilon_l)^{-1/N}) \quad (30)$$

with $\epsilon_l = 0.001$. The latter is selected according to (28). Also, we will consider cases $K = N$, $K = N/2$, $K = N/4$, and $K = N/16$. The corresponding plots are summarized in Fig. 4. As we see, with $\kappa_l = 1$ setting, the algorithm mainly detects noise in low SNR (Fig. 4(e) - 4(h)) and overestimates the number of components in high SNR regime. With the adjusted threshold, the number of detections at low SNR is almost zero, yet when a component is detected, it corresponds to the actual multipath component with

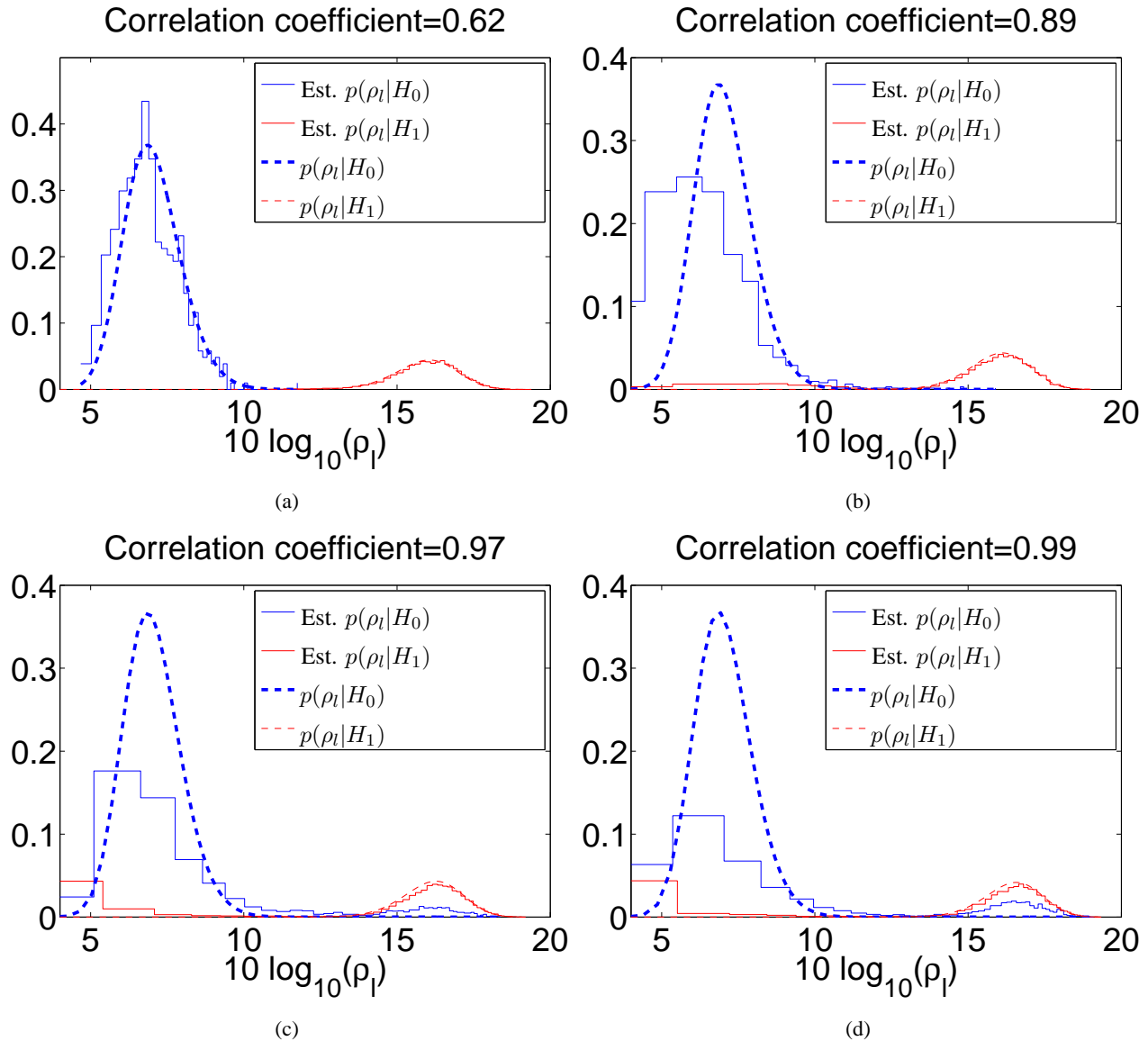


Fig. 3. Comparison of empirical and derived distributions of the test statistic ρ_l under H_0 and H_1 hypotheses for SNR= 17dB and a) $K = N/2$, b) $K = N/4$, c) $K = N/8$, and d) $K = N/16$.

high probability.

B. Superresolution properties of the algorithm

In the next simulation we investigate the resolution ability of the proposed IARD algorithm for both the assumptions A1 (IARD-A1) and the assumption A2 (IARD-A2). Here we will consider the case $L = 2$, with component delays τ_l no longer restricted to a sampling grid. Additionally, we will consider a Doppler shift ν_l for each component. This setting will correspond to a time-varying SISO channel model

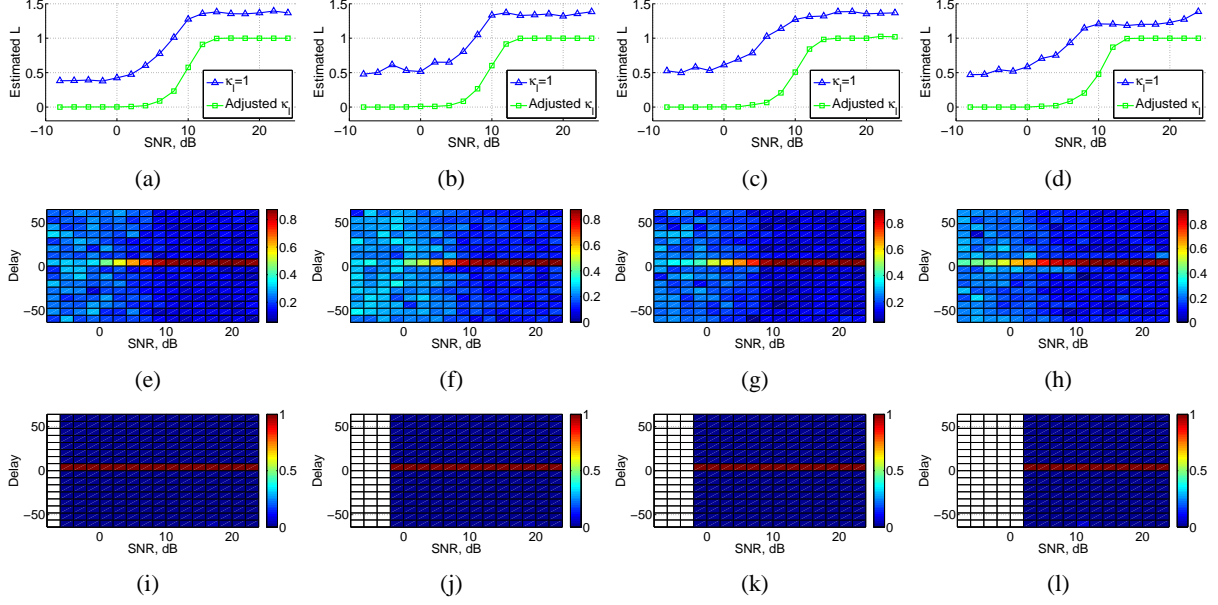


Fig. 4. Estimated number of components versus SNR for (a,e,i) $K = N$, (b,f,j) $K = N/2$, (c,g,k) $K = N/4$, and (d,h,l) $K = N/16$. In figures (e)-(h) $\kappa_l = 1$; in figures (i)-(l) $\kappa_l = \log(1/\log(1 - \epsilon_l))^{-1/N}$ with $\epsilon_l = 0.001$.

with stationary parameters. To estimate Doppler frequency we will consider $M = 25$ consecutive channel measurements, so that the model of a single component $s(\theta_l)$ is represented as $s(\tau_l, \nu_l) = \text{vec}\{\mathbf{X}\}$, where \mathbf{X} is an $R \times M$ matrix and $[\mathbf{X}]_{r,m} = s[r - \tau_l/T_s]e^{j2\pi\nu_l r m T_s}$, $r = 0, \dots, R - 1$, $m = 0, \dots, M - 1$. The signal $s[n]$ is a downsampled version of the actual 10MHz-wide calibration signal used in the aeronautical channel measurement campaign [33]. The used sampling period is $T_s = 4\mu\text{s}$, which results in $R = 128$ samples per single channel measurement. The synthetic delays $\tau = [\tau_1, \tau_2]^T$ of the components are generated as follows: τ_1 is uniformly drawn from the interval $[0, T_s]$ and $\tau_2 = \tau_1 + \Delta \cdot T_s$, with Δ being a simulation parameter. The Doppler frequency ν_1 of the first component is drawn uniformly from the interval $[-200, 200]$ Hz; for the second component we select $\nu_2 = \nu_1 + \epsilon_\nu$, where ϵ_ν is a random jitter in the interval $[-2, 2]$ Hz. The weights of both components have unit magnitude and uniformly distributed phase drawn from the interval $[0, 2\pi]$. For both IARD-A1 and IARD-A2 we will select the threshold according to (30).

For comparison purposes we will also consider a classical SAGE algorithm [5] that employs Bayesian Information Criterion (BIC) [7] to select the model order. Two different implementations of the SAGE algorithm with BIC criterion are compared. The first implementation (SAGE-BIC-1) exploits the signal detection method based on the eigenstructure of the estimated signal covariance matrix [8]. This algorithm first estimates the correlation matrix of the input signal \mathbf{y} using $N = R \times M$ data samples; then, the

information-theoretic criterion is applied to the eigenvalues of the correlation matrix following the scheme described in [8]. This gives an estimate of the number of signals, which is then plugged in the SAGE algorithm to estimate signal parameters. The second implementation (SAGE-BIC-2) estimates several models with different number of components L using the SAGE algorithm as follows: it starts with the model order $L = 0$ and sequentially increases the model order until the minimum of the BIC criterium is achieved, each time fitting the model anew. The BIC criterion is evaluated as

$$\text{BIC}(L) = -\log \left(p(\mathbf{y} | \hat{\Theta}, \hat{\mathbf{w}}) \Big|_L \right) + \frac{8}{2} L \log(N)$$

for each possible value of L . Here $\log \left(p(\mathbf{y} | \hat{\Theta}, \hat{\mathbf{w}}) \Big|_L \right)$ is the value of the log-likelihood function evaluated at maximum, under assumption that the model order is L . The penalty factor $\frac{8}{2} L \log(N)$ arises as follows: penalization per single complex amplitude is $\log(N)$, and per additional unknown time/frequency shift is $\frac{3}{2} \log(N)$ (see [34] and [6] for more details). Note that in this realisation SAGE-BIC-2 requires fitting multiple models to find the minimum of the BIC criterion. It is thus computationally very inefficient for realistic channels, where L might range up to several tens of components and number of samples N is on the order $\sim 10^3 - 10^5$.

As the performance criteria we compute the averaged number of detected components \hat{L} , the probability of detecting exactly two components $P_D^{(L=2)}$, the averaged delay root median squared error (RMSeSE) $\text{RMSeSE}(\hat{\tau})$ normalized by the sampling period T_s , and Doppler RMSeSE $\text{RMSeSE}(\hat{\nu})$, normalized by the Doppler resolution $1/NT_s$. The latter two quantities are computed only for the cases when a correct number of components is detected. Note that at low SNR the component detection rate will also be low, which is why the median squared error is used instead of mean squared error. Additionally, we evaluate the averaged computation time per single algorithm run. The corresponding plots for SNR 5dB, 10dB, 20dB, and 30dB are summarized in Fig. 5. The results are obtained by averaging over 2000 independent Monte Carlo runs for the IARD-A1, IARD-A2, and SAGE-BIC-1 algorithms. The statistics for the SAGE-BIC-2 algorithm are averaged over 300 Monte Carlo runs.

In terms of the estimated number of components \hat{L} (Fig. 5(a)-5(d)), and probabilities of detection $P_D^{(L=2)}$ (Fig. 5(e)-5(h)), the IARD-A1, IARD-A2, and SAGE-BIC-2 algorithms perform quite well, with the latter offering a slightly better performance. The SAGE-BIC-1 algorithm performs in contrast quite poorly: it either underestimates the number of components in low SNR regime, or consistently overestimates the model order in the high SNR regime. Its performance also seems to be insensitive to the component spacing Δ . In contrast, the number of correct detection for the other algorithms grows as

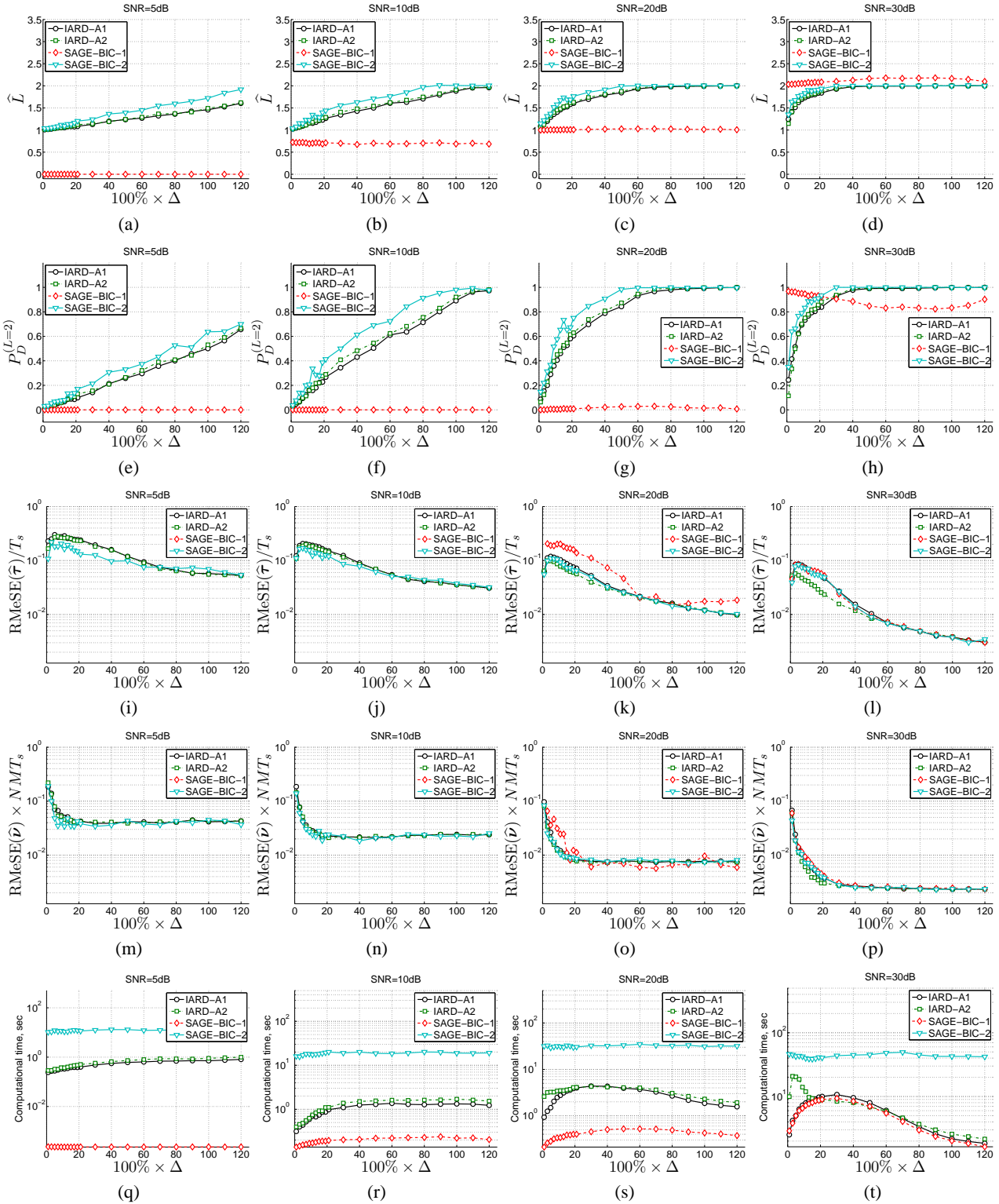


Fig. 5. Estimation performance of the algorithm in the superresolution regime for (a-e) 5dB, (f-j) 10dB, (k-o) 20dB, and (p-t) 30dB SNR. Shown are (a,f,k,p) the averaged number of detected components \hat{L} ; (b,g,l,q) the probability $P_D^{(L=2)}$ of the detecting exactly two components; (c,h,m,r) the normalized delay estimation RMSE, (d,i,n,s) the normalized Doppler estimation RMSE, and (e,j,o,t) the averaged computational time in seconds per single algorithm run.

Δ and SNR increases.

In terms of accuracy of parameter estimation (Fig. 5(i)-5(l) and 5(m)-5(p)) we see that in low SNR regime, SAGE-BIC-2 performs slightly better than the other algorithms. In the high SNR regime, SAGE-BIC-2 and IARD-A1 perform identically well, with IARD-A2 outperforming them for small component spacing Δ – the advantage of the assumption A2 over a “simpler” assumption A1. For larger spacing Δ , i.e., when the correlation between the components decreases, this advantage, however, disappears, and SAGE-BIC-2, IARD-A1 and IARD-A2 deliver similar performance.

Finally, let us consider the computational time of the algorithms (5(q) - 5(t)). It is interesting to note that although SAGE-BIC-2 has better component detection capabilities, its computational time is significantly higher, since multiple models with different number of components have to be estimated. SAGE-BIC-1 algorithm is the fastest, since the model order selection is done prior to multipath parameter estimation – the most time-consuming part of the algorithm. The IARD-A1 and IARD-A2 algorithms are much faster than SAGE-BIC-2, yet they offer a compatible performance both in terms of component detection probabilities, as well as in the parameter estimation accuracy. For a higher number of components L the inefficiency of the SAGE-BIC-2 algorithm will constitute itself quite significant.

The difference between the A1 and A2 assumptions exhibits itself only for component spacing Δ below approx. 60%, i.e., in a super-resolution regime. In terms of the detection rate, both assumptions perform quite similarly. As expected, the parameter estimation accuracy is better for the A2 assumption, yet at the expense of slightly higher computational time.

V. CONCLUSION

This work discusses a joint sparse estimation and detection of multipath components within variational Bayesian framework. The approach is based on a variational realization of incremental automatic relevance determination (IARD) algorithm – a Bayesian sparse signal reconstruction technique. The variational Bayesian formulation of the algorithm permits extending the standard IARD algorithm for linear models to a problem of parameters estimation of superimposed signals, which requires nonlinear optimizations. The sparsity is used to estimate the number of active signals in the model.

However, for the problem of super-resolution multipath component estimation, where an accurate model order selection is of a particular interest, it has been observed that IARD generally overestimates the number of components. Here we have demonstrated that this can be explained by the model fitting step at which dispersion parameters of propagation paths are estimated. This step performs a nonlinear optimization that adapts the dictionary matrix of the IARD algorithm. As a consequence, the model

overfits the measured signal and artifacts are inserted into the model.

To overcome this we proposed a hypothesis test that exploits statistical structure of the IARD inference expressions. We have shown that due to the optimization of multipath dispersion parameters, the corresponding sparsity parameters will follow an extreme value distribution under additive Gaussian noise assumption. This interpretation permits a correction of sparsity-driven model order selection within IARD using binary hypotheses testing. We have shown that the standard IARD approach is equivalent to a hypothesis test with a very high probability of false alarm, which explains model order overestimation. By adjusting the IARD pruning conditions to guarantee the desired false alarm probability, the model order selection can be improved and correct order can be estimated even in challenging super-resolution regime. Simulation studies have demonstrated that this adjustment allows extraction of the true signal sparsity in simulated scenarios and further acceleration of the convergence rate of the algorithm as compared to the classical information-theoretic model order selection schemes.

REFERENCES

- [1] J. Salmi, A. Richter, and V. Koivunen, "Detection and tracking of mimo propagation path parameters using state-space approach," *IEEE Trans. Signal Process.*, vol. 57, no. 4, pp. 1538–1550, Apr. 2009.
- [2] A. Richter, "Estimation of radio channel parameters : Models and algorithms," Ph.D. dissertation, Technische Universität Ilmenau, 2005.
- [3] T. Jost, W. Wang, D. Shutin, and F. Antreich, "Using an autoregressive model for DMC," in *Proc. 6th European Conf. Antennas and Propagation*, Prague, Czech Republic, Mar. 2012, pp. 3504 –3508.
- [4] H. Krim and M. Viberg, "Two decades of array signal processing research: the parametric approach," *IEEE Signal Process. Mag.*, vol. 13, no. 4, pp. 67–94, Jul. 1996.
- [5] B. Fleury, M. Tschudin, R. Heddergott, D. Dahlhaus, and K. I. Pedersen, "Channel parameter estimation in mobile radio environments using the SAGE algorithm," *IEEE J. Sel. Areas Commun.*, vol. 17, no. 3, pp. 434–450, Mar. 1999.
- [6] P. Stoica and Y. Selen, "Model-order selection: a review of information criterion rules," *IEEE Signal Process. Mag.*, vol. 21, no. 4, pp. 36–47, Jul. 2004.
- [7] A. Lanterman, "Schwarz, Wallace, and Rissanen: Intertwining themes in theories of model order estimation," *Int. Statistical Review*, vol. 69, no. 2, pp. 185–212, Aug. 2001.
- [8] M. Wax and T. Kailath, "Detection of signals by information theoretic criteria," *IEEE Trans. Acoust., Speech, Signal Process.*, vol. ASSP-33, no. 2, pp. 387–392, 1985.
- [9] M. Feder and E. Weinstein, "Parameter Estimation of Superimposed Signals Using the EM Algorithm," *IEEE Trans. Acoust., Speech, Signal Process.*, vol. 36, no. 4, pp. 477–489, Apr. 1988.
- [10] J. I. Myung, D. J. Navarro, and M. A. Pitt, "Model Selection by Normalized Maximum Likelihood," *J. of Mathem. Psychology*, vol. 50, pp. 167–179, 2005.
- [11] T. Jost, W. Wang, U. Fiebig, and F. Perez-Fontan, "Detection and tracking of mobile propagation channel paths," *IEEE Trans. Antennas Propag.*, vol. 60, no. 10, pp. 4875–4883, Oct. 2012.

- [12] C. Gentner and T. Jost, "Indoor positioning using time difference of arrival between multipath components," in *Proc. Indoor Positioning and Indoor Navigation (IPIN)*, Montbeliard, France, Oct. 2013, pp. 1–10.
- [13] M. J. Beal, "Variational algorithm for approximate Bayesian inference," Ph.D. dissertation, University College London, 2003.
- [14] C. M. Bishop, *Pattern Recognition and Machine Learning*. New York: Springer, 2006.
- [15] M. Tipping, "Sparse Bayesian learning and the relevance vector machine," *J. Machine Learning Res.*, vol. 1, pp. 211–244, Jun. 2001.
- [16] D. Wipf and B. Rao, "Sparse Bayesian learning for basis selection," *IEEE Trans. Signal Process.*, vol. 52, no. 8, pp. 2153 – 2164, Aug. 2004.
- [17] D. G. Tzikas, A. C. Likas, and N. P. Galatsanos, "The variational approximation for Bayesian inference," *IEEE Signal Process. Mag.*, vol. 25, no. 6, pp. 131–146, Nov. 2008.
- [18] D. Shutin and B. H. Fleury, "Sparse variational Bayesian SAGE algorithm with application to the estimation of multipath wireless channels," *IEEE Trans. Signal Process.*, vol. 59, no. 8, pp. 3609 – 3623, Aug. 2011.
- [19] D. Shutin, W. Wang, and J. Thomas, "Incremental sparse bayesian learning for parameter estimation of superimposed signals," in *Proc. 10th Int. Conf. Sampling Theory and Applications*, Bremen, Germany, Jul. 2013, pp. 513–516.
- [20] J. Fessler and A. Hero, "Space-alternating generalized expectation-maximization algorithm," *IEEE Trans. Signal Process.*, vol. 42, no. 10, pp. 2664–2677, Oct. 1994.
- [21] M. E. Tipping and A. C. Faul, "Fast marginal likelihood maximisation for sparse Bayesian models," in *Proc. 9th Int. Workshop Artificial Intelligence and Statistics*, Key West, FL, USA, Jan. 2003.
- [22] D. Shutin, T. Buchgraber, S. R. Kulkarni, and H. V. Poor, "Fast variational sparse Bayesian learning with automatic relevance determination for superimposed signals," *IEEE Trans. Signal Process.*, vol. 59, no. 12, pp. 6257–6261, Dec. 2011.
- [23] D. Shutin, S. R. Kulkarni, and H. V. Poor, "Incremental reformulated automatic relevance determination," *IEEE Trans. Signal Process.*, vol. 60, no. 9, pp. 4977 – 4981, Sep. 2012.
- [24] D. Shutin and T. Buchgraber, "Trading approximation quality versus sparsity within incremental automatic relevance determination frameworks," in *IEEE Int. Workshop on Machine Learning for Signal Processing*, Santander, Spain, Sep. 2012, pp. 1–6.
- [25] T. S. Rappaport, *Wireless communications. Principles and practice*. Prentice Hall PTR, 2002.
- [26] E. J. Candes, M. B. Wakin, and S. Boyd, "Enhancing sparsity by reweighted ℓ_1 minimization," *J. Fourier Analysis and Applications*, vol. 14, no. 5, pp. 877–905, Dec. 2008.
- [27] D. Wipf and S. Nagarajan, "A new view of automatic relevance determination," in *Proc. 21 Annual Conf. Neural Information Processing Systems*. Vancouver, British Columbia, Canada: MIT Press, Dec. 2007.
- [28] E. J. Candes, J. K. Romberg, and T. Tao, "Stable signal recovery from incomplete and inaccurate measurements," *Commun. Pure and Applied Mathematics*, vol. 59, no. 8, pp. 1207–1223, Aug. 2006.
- [29] R. A. Fisher and L. H. C. Tippett, "Limiting forms of the frequency distribution of the largest or smallest member of a sample," *Math. Proc. Cambridge Philosophical Society*, vol. 24, no. 02, pp. 180–190, Apr. 1928.
- [30] E. Gumbel, *Statistical theory of extreme values and some practical applications*, ser. Applied Math. U. S. Govt. Print. Office, 1954.
- [31] S. M. Kay, *Fundamentals of Statistical Signal Processing: Estimation Theory*. Upper Saddle River, NJ: Prentice Hall, 1993.

- [32] H. V. Poor, *An Introduction to Signal Detection and Estimation (2nd ed.)*. New York, NY, USA: Springer-Verlag, 1994.
- [33] N. Schneckenburger, D. Shutin, T. Jost, M. Walter, T. Thiasiriphet, A. Filip, and M. Schnell, “From L-band measurements to a preliminary channel model for APNT,” in *Proc. ION GNSS+ , to appear*, Tampa, FL, USA, Sep. 2014.
- [34] P. Djuric, “A model selection rule for sinusoids in white Gaussian noise,” *IEEE Trans. Signal Process.*, vol. 44, no. 7, pp. 1744–1751, Jul. 1996.